DESIGN OF PISTON DOF RESONANT-DRIVEN COMPLIANT MICRO-MIRROR

Milad Mesbahi
UCLA Mechanical and Aerospace Engineering
Los Angeles, CA, U.S.A.

ABSTRACT

This study delves into the development and optimization of a MEMS-based micro-mirror system, emphasizing its design, fabrication, and operational efficacy within advanced optical systems. Through the employment of the Freedom and Constraint Topologies (FACT) framework, creation of a twist-wrench mass and stiffness matrix, as well as Finite Element Analysis (FEA), a micro-mirror exhibiting a singular translational degree of freedom (DOF) orthogonal to its surface was synthesized. The design incorporates six thin wire flexures and two parallel plate actuators to achieve precise light modulation with minimal parasitic motion. Static analysis reveals a maximum displacement of roughly 125 micrometers, indicative of the system's robust performance. This paper outlines the systematic approach to the micro-mirror's design and the strategic fabrication process employed, highlighting the potential for contribution to research and development in adaptive optics, laser beam shaping, and optical communication systems.

INTRODUCTION

The quest for advanced optical systems has led to heightened demand for high-speed, high-precision micro-mirrors. These apparatuses are critical for a spectrum of high-impact applications that need to modulate light, including but not limited to adaptive optics, laser beam shaping, and optical communication systems. Micro-Electro-Mechanical-Systems (MEMS) based micro-mirrors have emerged as one of the cornerstone technologies in this domain due to the scale of its operation. Many of these MEMS devices offer unparalleled control over the light phase and direction, and based off of the system's design can translate and rotate along certain desired axes to achieve the desired modulations. An example of a basic MEMS micro-mirror and these concepts is shown in Figure 1.

A significant body of research has focused on new MEMS design configurations and various actuation methods that enhance the performance of these micro-mirrors. Resonant-driven micro-mirrors are of particular interest, since operating at the system's resonant frequency can significantly reduce the required actuation energy and thus greatly simplifies the control mechanisms required. This negation of the need for complex sensor feedback or closed-loop control circuitry to reach desired operation speeds has been explored through various studies and

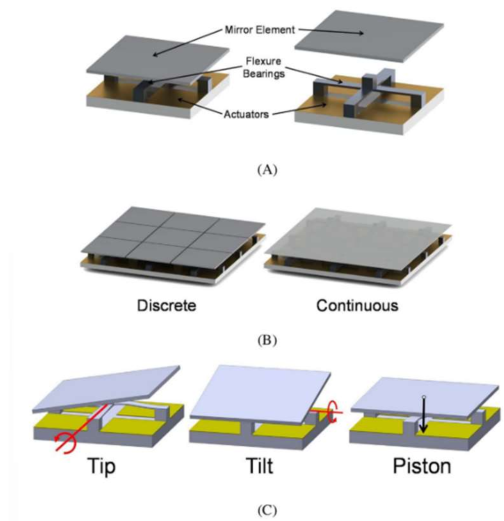

FIGURE 1: ILLUSTRATIVE MICROMIRROR CONFIGURATION (A); COMPARISON BETWEEN DISCRETE AND CONTINUOUS MIRROR SURFACES IN A TWO-DIMENSIONAL MICRO-MIRROR ARRAY (B); DEGREES OF FREEDOM (DOFS) IN MICROMIRRORS ESSENTIAL FOR DIRECTING OR MODULATING LIGHT PHASE (C).

is based on the underlying principle of maximizing the natural frequency of the mirror's desired translational degree of freedom [1-2]. By doing so, the system can facilitate high-speed operation while also ensuring that the other modal behaviors of the system are substantially higher (> 10x) to prevent unwanted modal interactions that could lead to parasitic errors [3].

Facilitating these operational dynamics is not a simple task, as these devices must often balance between swift response, range, and maintaining high precision in light modulation. Furthermore, it often requires engineers to finely tune the mechanical properties of a given micro-mirror to achieve this balance, whether it be through specific material selections or structural design manipulations. Materials with high stiffness-to-density, often employed in MEMS fabrication, can lead to high natural frequencies while also maintaining structural integrity [4-5].

Actuation mechanisms can help drive the motion at these resonant frequencies, amplifying the range and duration in which these micro-mirrors translate. Popular actuators include electrostatic, electromagnetic, piezoelectric, and bimorph actuators, each with their unique benefits and limitations. Electrostatic actuation has been widely adopted for numerous applications due to its simplicity and low power consumption, although challenges have arisen due to issues with the pull-in instability limiting its effective stroke [4-5]. Conversely, piezoelectric actuators offer larger strokes and precise control but can often be hampered with issues like hysteresis and larger form factors, making them less ideal for applications requiring compactness and rapid response [6-7]. This study will focus on parallel plate, as shown in Figure 2 and detailed later.

The design and fabrication processes employed also play a very important role in achieving the desired natural frequencies. Since MEMS devices operate on microscopic scales that range from one micrometer to several millimeters, advanced fabrication techniques are needed. These can include innovative technologies like Deep Reactive-Ion Etching (DRIE) and surface micromachining, which enables us to create very intricate micro geometries with unparalleled precision. DRIE in particular is known for its ability to produce highly anisotropic etch profiles, which has been used in more sophisticated systems [8-9]. In this particular study, our flexure-system is relatively simple enough to use standard microfabrication procedures such as photolithography to accurately pattern the micro-mirror and the critical thin wire flexures.

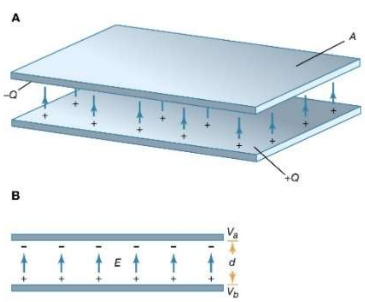

FIGURE 2: PARALLEL PLATE ACTUATOR CONCEPT

TOPOLOGY SYNTHESIS

In the development of the micro-mirror system designed and discussed in this paper, which exhibits a singular translational degree of freedom (DOF) orthogonal to the mirror's surface, the Freedom and Constraint Topologies (FACT) framework was employed to achieve a topology synthesis that precisely aligned with the desired motion characteristics. FACT methodology, as taught by UCLA Professor Jonathan Hopkins, is rooted in the principles of constraint-based design and utilizes screw theory and projective geometry to articulate all the possible freedom and constraint spaces within which any mechanism can operate within [10]. With this approach, an exhaustive enumeration of potential flexure systems can be designed by linking specific motions (freedom topologies) to the flexure elements (constraint topologies) that guide them. A copy of a FACT chart for parallel flexure systems is shown in Figure 2 for reference.

It is important to begin the design process with a clear defintiion of the desired motion, which in this case, was a straightforward translation orthogonal to the mirror's surface.

As seen in Figure 3, 1 DOF type 3 has a constraint space of stacked blue planes to achieve a black translation arrow. Not

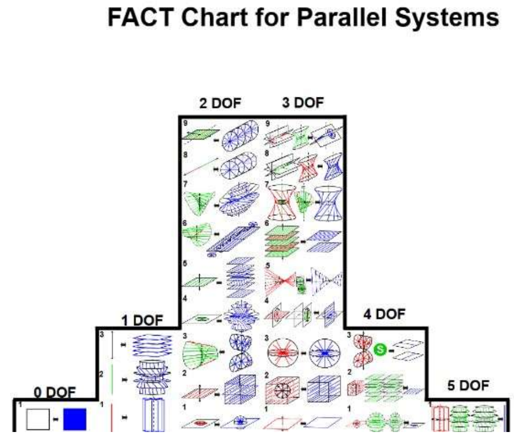

FIGURE 2: FACT CHART FOR PARALLEL SYSTEMS – 1 DOF TYPE 3 DESIRED

only does our design need to replicate this constraint space of parallel planes in series, but it should also do so with as few elements as possible. Using Maxwell's equation,

$$6 - R = C \tag{1}$$

Where R is the number of degrees of freedom desired and C is the number of constraints needed to accomplish this [11]. 6 represents the maximum number of degrees of freedom any system can achieve in 3-Dimensional space (3 translations, 3 rotations). In this case, R is 1 (1 DOF type 3) and thus our C is 5.

With this constraint topology in mind and the number of elements needed, the following parallel flexure system was synthesized as shown in Figure 3.

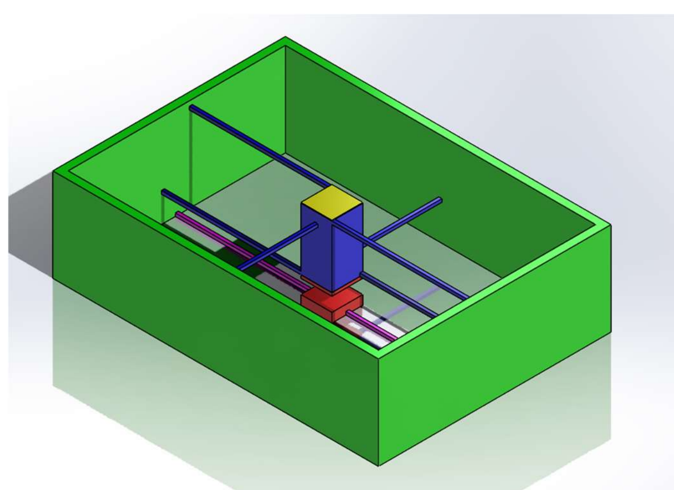

FIGURE 3: CAD DEPICTION OF FLEXURE-BASED SYSTEM: YELLOW – MIRROR SURFACE, PURPLE – STAGE/STAGE WIRES, RED – PARALLEL CAPACTIANCE PLATES, GREEN – GROUND, PINK – GROUND WIRE FLEXURES.

To ensure a robust design, thin wire flexures, with cross-sectional dimensions of 0.1mm^2 and lengths varying between 3mm and 4.5mm, were utilized. The stage's dimensions were kept congruent with the required surface area of 1mm^2 of the micro-mirror. The micro-mirror has a thickness of 0.1mm, which seemed to be consistent with other papers that use resonating micromirrors [12]. All of these dimensions were rigorously optimized through Finite Element Analysis (FEA) simulations, which confirmed that these specific values yielded the most favorable mode shapes, aligning with the system's functional requirements.

The system consists of six total flexure elements, with numerous planes offset to increase the overall range of the system. This offset was amplified by increasing the height of the micro-mirror's stage, which required numerous trial and error to strike a balance between the desired mass of the stage and the range in which the system can achieve through maximum offset of these parallel planes.

The decision was made to create a parallel flexure system over similar serial or hybrid configurations. This can be explained for numerous reasons. Firstly, parallel flexure systems are characterized by their inherent stiffness and high precision due to the simultaneous action of multiple flexures that support the load. Serial and hybrid systems, in contrast, are often more susceptible to parasitic rotations and displacement due to the cumulative effect of compliance in each successive flexure element. Secondly, this parallel system, which consists solely of wire flexures, allows for a more uniform distribution of loads across flexure elements, reducing the risk of localized stress concentrations that might lead to premature failure. Since the load is transferred sequentially through the flexures in serial and hybrid systems, wear and fatigue might be exacerbated in comparison to this parallel system. Lastly, the dynamic performance and overall compactness of the design contribute to lower required actuation forces and manufacturing feasibility. It makes the modelling much simpler, especially when coupled with the use of rectangular geometries for all wire flexures used and stages.

Although Equation 1 shows that only five constraints are necessary for this, the system contains six total constraints. This approach, while seemingly counterintuitive, is aimed at ensuring symmetry and enhancing the structural integrity of the micro-mirror system., and thus addresses several key design challenges. Symmetry is particularly important to minimize undesired motions and vibrations, and an asymmetrical design could introduce bias in the flexure system's response to loads, resulting in non-uniform deformations. This design in Figure 3, as later corroborated by both Stiffness-Matrix calculations on MATLAB and a frequency analysis performed on SolidWorks, the addition of this order of constraint of one ensured uniform stress distribution and consistent performance across the micro-mirror's operational range.

SYSTEM ACTUATION

The design incorporated in this study opts for parallel plate actuators, and the placement of these plates are depicted in Figure 3 in red. Each plate replicates the surface dimensions of 1mm^2 of both the stage and micro-mirror, making it easy to assemble. Both capacitance plates (one is attached to the bottom of the stage and the other is attached to ground) are directly parallel with one another and a certain gap D away. An electrostatic force is generated between two parallel plates of Aluminum 1100 O-Rod, which was chosen due to its highly conductive alloy of aluminum.

The use of plate actuators in over half of existing MMA designs and here as well can be attributed to several advantages: they are compact, offer rapid response to voltage changes, generate minimal heat, consume low power, provide a direct correlation between voltage and actuation force, and are relatively simple to fabricate. Furthermore, since their force density increases as the device size decreases, making them particularly effective in MEMS applications like this [13].

Although there are numerous limitations to parallel plate actuators, many of these are eliminated due to the simplicity of our design and the piston-type motion that is desired. For instance, the fact that the plate actuators are unipolar, meaning they are capable only of pulling the plates together and not pushing them apart, isn't necessarily a problem in this case since the system is resonant-driven and only needs its motion amplified in the single degree of freedom specified.

However, an important concept to note when determining the gap d between the parallel plates is the effect of pull-in behavior. This phenomenon is caused when excessive force due to too small of a gap distance causes the plates to collapse into contact, potentially leading to short circuits. It is primarily governed by the relationship between electrostatic and mechanical forces in a system where a mass is suspended by a spring with stiffness k, across a gap, and is captured by Equation (2):

$$V_{app} = V_p = \sqrt{\frac{8}{27}\frac{kd^3}{\varepsilon_0 A}} \tag{2}$$

Here, V_{app} represents the applied voltage across the gap, inducing a capacitive effect and an electrostatic force counteracted by the spring's force, while V_p represents the threshold at which the electrostatic force surpasses the spring's resistance. This voltage marks the boundary between stable operation and the risk of pull-in instability and thus Equation 2 serves as a fundamental guide for optimizing the actuator's geometry and material properties.

DESIGN CHARACTERIZATION

TABLE 1: COMPARISON OF NATURAL FREQUENCIES BASED OFF INDEPENDENT CALCULATION METHODS

Mode #	FEA (Hz)	Stiffness Matrix (Hz)
1	2,519.2	2,607.6
2	33,935.0	39,414.8
3	34,295.0	48,586.0
4	34,482.0	59,379.7
5	34,542	94,434.6

Table 1 describes the first five calculated mode shapes from using both the generated twist-wrench and stiffness matrix and the FEA analysis results. The first two modes are typically simpler, involving more global and less complex deformations of the structure and can therefore be closely approximated by both FEA and stiffness matrix calculations, resulting in similar natural frequencies within acceptable ranges (3.5% difference for the 1st mode, 16% difference for 2nd mode). As the mode shapes become more complex (modes 3-5), the FEA, which accounts for detailed geometric and material property variations, might capture smaller complexities due to the fineness of the mesh, which are not fully encapsulated in the stiffness matrix method, leading to the displayed larger discrepancies.

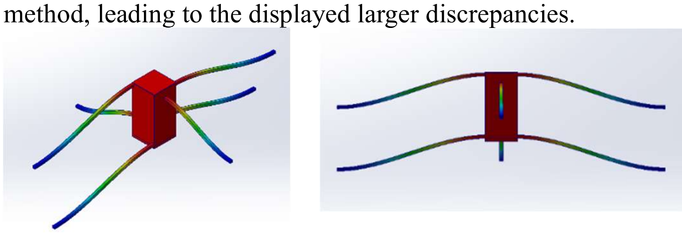

FIGURE 2: FIRST MODE I) TOP VIEW II) SIDE VIEW

Figure 4 depicts the motion of the first mode, which as explicitly seen in the side view, exhibits the piston-type DOF.

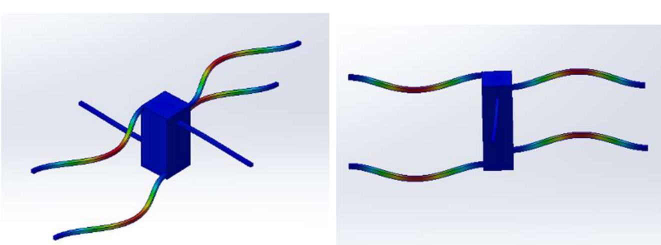

FIGURE 5: SECOND MODE I) TOP VIEW II) SIDE VIEW

The translation moves with virtually no tip or tilt, exemplifying the robustness of the model and removal of unwanted motion. The second mode, which is about 15.11 times higher than the first mode and shown in Figure 5, is when we finally begin to see buckling and motion along different axes, which is not desired for our study. However, because of the large gap between the first and second modes, which was carefully optimized after numerous different design and parameters changes, this dynamic behavior at higher mode shapes is largely avoidable.

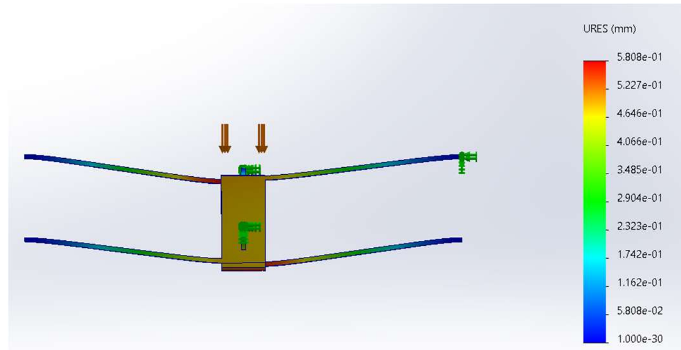

FIGURE 6: DISPLACEMENT UNDER LOADING

As shown in Figure 6, a static analysis was also conducted to determine the range of our micro-mirror setup. Efforts were focused on identifying optimal force values that facilitate pure translation while maintaining stresses within the wire flexures at less than 20% of their yield strength, which can be calculated by understanding the yield stress of single-crystalline silicon at room temperature is approximately 7-10 GPa for reference [14]. This analysis, along with numerous additional ones, demonstrated a notable maximum displacement of roughly 125 micrometers without inducing significant strains on either the wire flexures or the stage. This displacement is consistent with the performance of existing micro-mirror systems, indicating a robust design capable of meeting operational demands.

Although these are merely rough results, they are promising and indicative of the benefits of using FACT to design flexure-based systems for MEMS applications. Further adjustments in design parameters and material selection are anticipated to increase this displacement potential, aligning with objectives to refine the system's efficacy in applications necessitating precise optical modulation.

FABRICATION APPROACH

Below is a concise, scientific explanation of each fabrication step and its rationale. To start off, silicon wafers are chosen for their excellent mechanical stability and compatibility with standard MEMS fabrication techniques. The wafer undergoes a rigorous cleaning protocol to remove surface contaminants, ensuring the integrity of subsequent fabrication steps. We can follow this step and use UV photolithography with positive photoresist to facilitate the accurate transfer of micro-mirror and flexure designs onto the silicon substrate. Next, we can implement the Bosch process, employing DRIE to etch the silicon wafer, creating the 3mm-4.5mm long wire flexures and the 1 mm² stage. DRIE has a unique ability to produce vertical sidewalls and high-aspect-ratio features, which resulted in its selection as a microfabrication method used here due to the required precise dimensions of the flexures and stage.

Following the etching process, aluminum is sputtered to form the two 1 mm² by 0.3mm thick capacitance plate beneath the silicon stage and ground. This step also involves depositing a thin layer of silicon on the top surface of the silicon stage to form the micro-mirror. The choice of silicon for the micro-mirror is due to its excellent reflectivity and compatibility with MEMS devices. Lastly, we can finish off by etching away parts of the sacrificial layer or the substrate itself to release the wire flexures and allow for free movement of the silicon stage and the attached micro-mirror. The process is carefully controlled to prevent damage to the micro-mirror and the flexures.

CONCLUSION

This study successfully demonstrated the design, optimization, and fabrication of a MEMS-based micro-mirror system, achieving a singular translational degree of freedom (DOF) essential for small-scale optical applications. Utilizing the Freedom and Constraint Topologies (FACT) framework, MATLAB Stiffness models, and Finite Element Analysis (FEA), the design incorporates thin wire flexures and parallel plate actuators to facilitate precise light modulation. Static analysis confirmed a robust displacement capability of roughly 125 micrometers, highlighting the system's potential for high precision without structural compromise.

The selection of parallel plate actuators over its counterparts underscored the system's efficient actuation, which we tailored for rapid response and minimal power consumption. Fabrication processes, from substrate preparation to the detailed etching and deposition steps, were explained in detail. Future optimizations with regard to the design parameters and materials promise to further enhance the system's displacement and precision.

ACKNOWLEDGEMENT

I would like to thank Professor Jonathan Hopkins and TA Talmage Jones for their knowledge and guidance through MAE C162B and introduction in FACT based design.

REFERENCES

[1] Dudde, Ralf, Shanshan Gu-Stoppel, Ulrich Hofmann, Dirk Kaden, Quenzer H.-J., Vanessa Stenchly and Bernhard Wagner. “New Designs for MEMS-Micromirrors and Micromirror Packaging with Electrostatic and Piezoelectric Drive.” (2016).

[2] Hu, Fangrong, Jun Yao, Chuankai Qiu and Hao Ren. “A MEMS micromirror driven by electrostatic force.” Journal of Electrostatics 68 (2010): 237-242.

[3] Fangrong Hu, Jun Yao, Chuankai Qiu, Hao Ren. "A MEMS micromirror driven by electrostatic force." (2010): Journal of Electrostatics, Volume 68, Issue 3, Pages 237-242, ISSN 0304-3886, https://doi.org/10.1016/j.elstat.2010.01.005.

[4] Dagel, Daryl & Cowan, William & Spahn, Olga & Grossetete, Grant & Grine, Alejandro & Shaw, Michael & Resnick, Paul & Jr, B.. (2006). Large-Stroke MEMS Deformable Mirrors for Adaptive Optics. Microelectromechanical Systems, Journal of. 15. 572 - 583. 10.1109/JMEMS.2006.876794.

[5] Steven A. Cornelissen, Paul A. Bierden, Thomas G. Bifano, Charlie Lam V. Lam, "4096-element continuous face-sheet MEMS deformable mirror for high-contrast imaging," J. Micro/Nanolith. MEMS MOEMS 8(3) 031308 (1 July 2009) https://doi.org/10.1117/1.3158067

[6] Zamkotsian, Frederic, Severin Waldis, Wilfried Noell, Kacem ElHadi, Patrick Lanzoni and Nico F. de Rooij. “Micro-mirror array for multi-object spectroscopy.” SPIE Astronomical Telescopes + Instrumentation (2006).

[7] Piyawattanametha, Wibool, Pamela R. Patterson, M. S. Wu, Dooyoung Hah and Hiroshi Toshiyoshi. “A surface and bulk micromachined angular vertical combdrive for scanning micromirrors.” OFC 2003 Optical Fiber Communications Conference, 2003. (2003): 251-252 vol.1.

[8] Ersumo, N.T., Yalcin, C., Antipa, N. et al. A micromirror array with annular partitioning for high-speed random-access axial focusing. Light Sci Appl 9, 183 (2020). https://doi.org/10.1038/s41377-020-00420-6

[9] Ankur Jain, Hongwei Qu, Shane Todd, Huikai Xie. "A thermal bimorph micromirror with large bi-directional and vertical actuation." Sensors and Actuators (2005) ISSN 0924-4247, https://doi.org/10.1016/j.sna.2005.02.001.

[10] Hopkins, Jonathan B. “Design of Parallel Flexure Systems via Freedom and Constraint Topologies (FACT).” Design of Parallel Flexure Systems via Freedom and Constraint Topologies (FACT), 2007.

[11] Hopkins, J. B. (n.d.). Lecture 4: Compliant Mechanism Design Theories. MAE C162B/C294A Course. Los Angeles; CA.

[12] Farrugia, Russell & Grech, Ivan & Camilleri, Duncan & Casha, Owen & Gatt, E. & Micallef, Joseph. (2018). Theoretical and finite element analysis of dynamic deformation in resonating micromirrors. Microsystem Technologies. 24. 1-11. 10.1007/s00542-017-3335-7.

[13] Afrang, Saeid & Mobki, Hamed & Hassanzadeh, Malek & Rezazadeh, Ghader. (2019). Design and simulation of a MEMS analog micro-mirror with improved rotation angle. Microsystem Technologies. 25. 10.1007/s00542-018-4083-z.

[14] Mueller, M.G., Žagar, G. & Mortensen, A. Stable room-temperature micron-scale crack growth in single-crystalline silicon. Journal of Materials Research 32, 3617–3626 (2017). https://doi.org/10.1557/jmr.2017.238

